CHALMERS
UNIVERSITY OF TECHNOLOGY

Remote Sensing of Road-Surface Condition Using a 77–81 GHz Polarimetric Radar

Downloaded from: https://research.chalmers.se, 2026-07-17 08:48 UTC

Citation for the original published paper (version of record):
Vassilev, V., Kälvesten, A., Kalmnäs Drakenfors, N. (2026). Remote Sensing of Road-Surface Condition Using a 77–81 GHz Polarimetric Radar. Journal of Infrared, Millimeter, and Terahertz Waves, 47(7). http://dx.doi.org/10.1007/s10762-026-01155-y

N.B. When citing this work, cite the original published paper.

research.chalmers.se offers the possibility of retrieving research publications produced at Chalmers University of Technology. It covers all kind of research output: articles, dissertations, conference papers, reports etc. since 2004. research.chalmers.se is administrated and maintained by Chalmers Library

(article starts on next page)

Journal of Infrared, Millimeter, and Terahertz Waves (2026) 47:48
https://doi.org/10.1007/s10762-026-01155-y

RESEARCH

Remote Sensing of Road-Surface Condition Using a 77–81 GHz Polarimetric Radar

Vessen Vassilev[1,2] · August Kälvesten[1,2] · Nils Kalmnäs Drakenfors[1]

Received: 5 February 2026 / Accepted: 23 June 2026
© The Author(s) 2026

Abstract

We present a detection method and measurements of low-friction formations on road surfaces using a monostatic polarimetric radar installed on a vehicle in motion. Polarimetric parameters (PP) such as entropy, depolarization, and the proportion of surface-scattering are used to identify the surface and classify it as dry, wet, or icy. The polarimetric parameters are calculated from the eigenvalues (EV) of the measured covariance/coherence matrix. Due to the low contrast in the polarimetric parameters between icy and dry surfaces, the classification of the surface becomes challenging in the presence of irregularities on the surface that can be interpreted as ice. To minimize the false alarms, in addition to the PP, we use the sum of the non-normalized eigenvalues, which is a measure of the total scattered power in all polarization components. The sum of the EV has better contrast compared to the PP and helps in reducing the negative effect of natural surface irregularities. To classify the surface, we calculate the adaptive mean value and variance of the PP and non-normalized EV and compare each measurement to a threshold. The surface is classified after a certain combination of parameters exceeds their threshold value. We demonstrate how each of the parameters is affected by an icy/wet surface compared to the same surface in dry conditions. In our measurements, we are able to detect ice patches with a false alarm below 2% with a simple classification criterion combining some of the PP with the sum of the EV.

Keywords Radar polarimetry · Road surface identification · Black-ice · Target entropy · Distributed target · mm-wave radar · Automotive radar

✉ Vessen Vassilev
vessen.vassilev@chalmers.se

August Kälvesten
august.kalvesten@saabgroup.com

Nils Kalmnäs Drakenfors
nilskal@student.chalmers.se

[1] Department of Microtechnology and Nanoscience (MC2), Chalmers University, Kemivägen 9, Gothenburg 41296, Sweden

[2] VVWaves AB, Lindome 43734, Sweden

Published online: 03 July 2026

1 Introduction

A sensor capable of analyzing properties of the road surface in front of a moving vehicle can assist the driver or the control system of the car in detecting sections of the road with reduced friction. Of particular interest are condensed moisture or wet areas in the process of freezing, resulting in formations such as thin (black) ice, which might be visually indistinguishable.

Previous studies to detect ice formations on road surfaces include a 61 GHz bistatic polarimetric radar sensor capable of distinguishing various types of surfaces under a moving vehicle, as presented in [1], and a 24 GHz monostatic sensor [2], [3], both measuring backscattering coefficients for vertical, horizontal, and cross polarizations. In these studies, the surfaces are characterized through their polarimetric backscatter coefficients or their ratios and thus do not consider the random nature of the road surfaces as a distributed target.

For a sensor mounted on a moving vehicle, every measurement is performed on a different section of the surface. Due to the random nature of road surfaces, a single measurement is not sufficient to extract reliable information about the properties of the surface. Therefore, a statistical approach has to be adopted. Such a method has been developed for polarimetric synthetic aperture radar (SAR) observations [4] and has been used to classify surfaces of various types, identify frozen areas [5], and measure roughness of road surfaces from airborne observations [6]. In this work, we do not use any sort of SAR processing, but we use the same decomposition of the coherence matrix and interpretation of the eigenvalues as used in the case of polarimetric SAR.

Our prior work shows that $entropy(H)$ and $polarimetric - pedestal(P_H)$, also called $depolarization$, can be used to identify whether the surface is wet, dry, or ice-covered. In [7], through laboratory measurements, we show that compared to dry-surface ice-covered surface increases both entropy and depolarization, while in wet conditions these two parameters decrease. A combination of entropy and auxiliary angle α is used to distinguish freezing and thawing states of surfaces [5]. Fully polarimetric measurements of surface scattering using a laboratory instrument are presented in [11] for road surfaces under various conditions. In [8], H-α is measured on different types of road surfaces and conditions from a vehicle in motion. We showed how varying surface roughness affects H, P_H, and α. In addition to the alternating roughness, the fact that the radar beam penetrates into the surface and the presence of various irregularities on road surfaces, such as marking lines and potholes, produce variations in the measured PP and make the detection of black-ice areas challenging.

In this manuscript, we present for the first time measurements of thin-ice-covered road surfaces from a vehicle in motion. We compare the polarimetric parameters (PP) between dry, icy, and wet surfaces and show that wet areas produce high contrast in all PP. Icy-covered surfaces, on the other hand, are more difficult to detect due to the lower level of contrast between dry-asphalt and ice—a result of the similarity in their dielectric constants [12]. The presence of irregularities in the structure of the road makes the detection of ice challenging if only a single PP is used to classify the surface.

The number of runs is recorded for different radar configurations and angles of incidence. In the following sections, we present two examples when the radar shifts from dry to icy and dry to wet surfaces. We show the influence on the polarimetric parameters and how they are affected by the properties of the surface.

Examining all PP, we conclude that the sum of the non-normalized eigenvalues (EV) is the quantity that produces the highest contrast between the different surfaces and is less prone to fluctuations due to irregularities. We therefore use non-normalized EV in combination with entropy or depolarization to minimize false alarms. To classify the surface, we calculate the adaptive mean value and variance of the PP and non-normalized EV to set a detection threshold. We compare the current value to the threshold, which is continuously updated based on past measurements over a specific time interval. The surface is classified when a certain combination of parameters exceeds their threshold values. In our measurements, we are able to demonstrate detection of ice patches with a false alarm below 2%, wet patches are detected error-free with an FA of 0%.

2 Measurements Setup

A test vehicle, equipped with a 77–81GHz polarimetric radar and a video camera, drives over the ice patches with a constant speed in the range of 3–8 m/s as shown in Figs. 1 and 2. The radar sensor is based on the AWR 1843 chipset from TI and uses 2 transmitters and 2 receivers to measure the [S] scattering matrix from Eq. 1. All transmitters and receivers are coupled to a single conical horn antenna. A waveguide polarization filter separates/combines the H and V components into orthogonal rectangular waveguides connected to the corresponding transmitter/receiver.

The radar H and V receivers are producing IQ data, which, after applying calibration corrections, are converted to complex scattering parameters S_{HH}, S_{VV}, and S_{HV}. The $S - parameters$ are calibrated using a sphere as a reference target. S_{HH} and S_{VV} are corrected to attain the same magnitude and range. The S_{HV} parameter was found to be 17 dB below the co-pol components, which is below the cross-pol produced by the road-surface and thus is not amplitude corrected. To verify the cross-pol component S_{HV} produced by the radar hardware, we also used a rotating dihedral at three positions: horizontal, vertical, and at 45°. For the latter, we verify that the cross-pol component amplitude is the same as the co-pol components at H and V orientations of the dihedral.

More details on the radar hardware can be found in [8]. The radar beam is pointed forward as shown in Fig. 3 and shifts from dry to icy and back to dry surface several times in each test. A video camera is located next to the radar and is pointed at the area on the surface, which is illuminated by the radar beam. The purpose of the camera is to verify the time instances when the vehicle is entering a patch of ice or a wet surface. The video sequence is used to relate the PP measured by the radar to the actual condition of the surface.

On one occasion, the ambient temperature became positive, the ice melted and partially evaporated. The amount of water was sufficiently small and did not cover the surface. Thus, we could collect data from the same ice patches but in wet conditions. However, we do not have a measurement run that combines wet, dry, and icy patches. The two examples presented in the following section are for separate measurements on dry-icy and dry-wet surfaces.

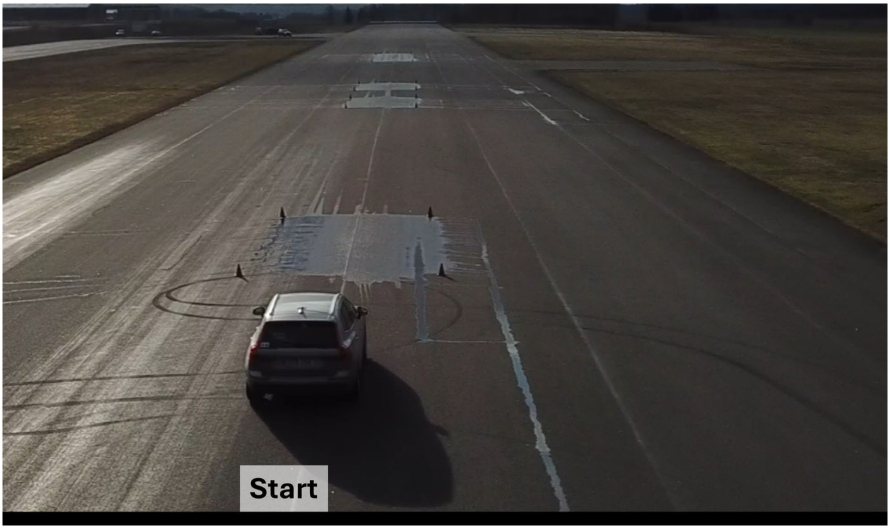

Fig. 1 Picture of the testing site. Thin (1–3 mm) ice patches are created by spraying water at negative temperatures and thus emulating black-ice conditions. A polarimetric radar sensor mounted on a test vehicle provides data in real time. A video camera collects data to match the radar measurements to the actual state of the surface while driving along the patches

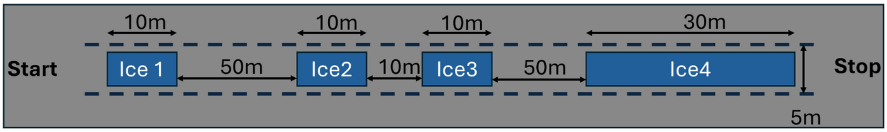

Fig. 2 Schematic of the size and location of the ice patches

Table 1 Chirp configuration

Time between [S] measurement *ms*	Num. of samples for 1 chirp	Sampling rate *MHz*	Max range *m*	Range resolution *mm*
25	64	5	5.2	83

Table 2 Main measurement parameters for dry/icy surfaces

	Angle of incidence θ_i, *deg*	Range to the surface *m*	Covered surface area L/W, *m*	Vehicle speed m/s	Num. [S] measurements used for PP estimation
Dry-icy	60	3.2–3.7	0.54/0.27	3.4	70
Dry-wet	40	2–2.5	0.23/0.18	8.3	40

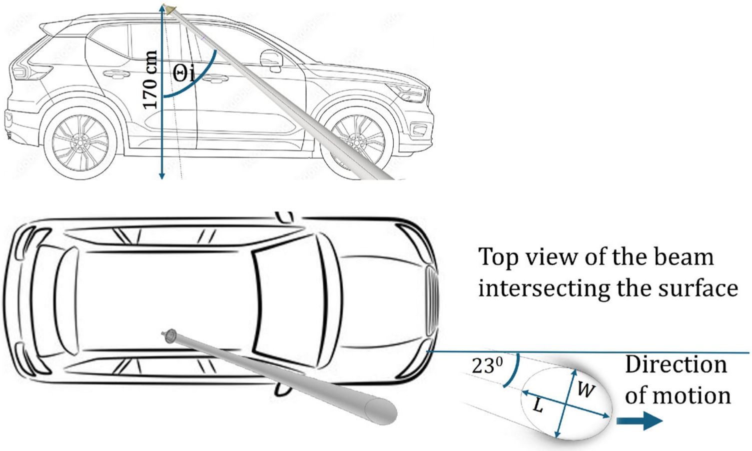

Fig. 3 Radar placement on the vehicle

Some of the main parameters of the radar configuration are summarized in Table 1. The radar measures the polarimetric scattering matrix $[S]$ and sends it to a computer every 25 ms. The PP are calculated based on the current and a number of previous $[S]$ measurements and are displayed in real time. As shown in Table 2 for the Dry-Wet surface, we use 40 $[S]$ measurements for each estimation of the PP. As the $[S]$ matrix arrives every 25 ms, each PP covers measurements over a 1-s interval. A larger number of $[S]$ measurements results in less variation in the PP caused by the natural irregularities of the surface.

The cross-section between the radar beam and the road surface is an elliptical shape as shown in Fig. 3. The geometry and some of its main attributes are summarized in Table 2.

3 Polarimetric Parameters of Dry, Ice-Covered, and Wet Surfaces

The method used to estimate the PP is described in detail in [7] and [8]. Here, we summarize the calculation of the main polarimetric parameters and how they are affected by the condition of the surface.

The input for the calculation of the coherence matrix is the measured scattering matrix, which is defined as:

$$\begin{bmatrix} S_{VV} & S_{VH} \\ S_{HV} & S_{HH} \end{bmatrix} \tag{1}$$

where the first index indicates the polarization of the transmitter and the second the polarization orientation of the receiver. The reciprocity theorem of backscattering states that $S_{HV} = S_{VH}$. An example of received S-parameters is shown in Fig. 4 where the surface covers range between 3.2 and 3.7m.

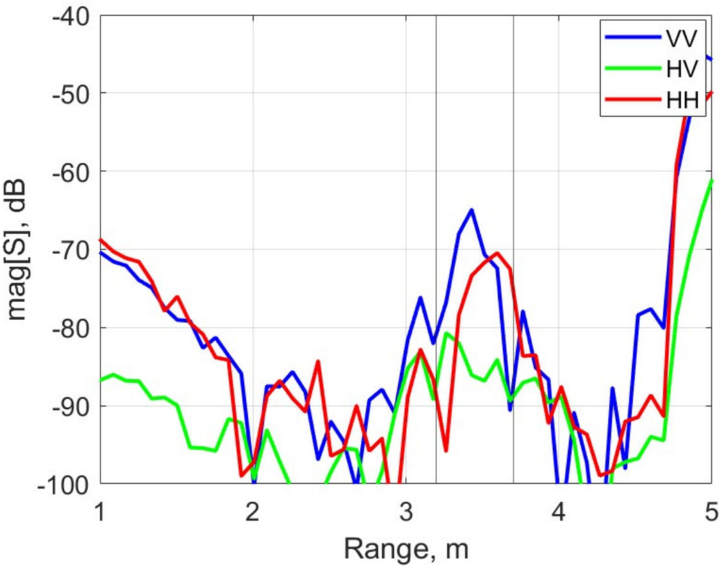

Fig. 4 Magnitude of the polarimetric S-parameters for a non-moving vehicle. The S-parameters are measured and communicated each 25 ms. The surface response is visible for a range between 3.2 and 3.7m and is marked with vertical lines. The high values of $|S|$ for ranges <2 m and >4.5m are caused by reflections within the radar hardware

The coherence matrix T can be represented as the product of the coherence vector k with its transposed complex conjugate [4] and contains *3x3* elements:

$$T = kk^{\dagger} \tag{2}$$

where the coherence/scattering vector k is given by:

$$k = \begin{bmatrix} S_{HH} + S_{VV} \\ S_{HH} - S_{VV} \\ 2S_{HV} \end{bmatrix} \tag{3}$$

To calculate the eigenvalues and eigenvectors of the coherence matrix, a minimum of 3 measurements is needed. For a set of N number of measurements, the measurement matrix M consists of N columns of the measured coherence vector in the presence of noise.

$$M = \begin{bmatrix} | & | & .. & | \\ k^1 & k^2 & .. & k^N \\ | & | & .. & | \end{bmatrix} \tag{4}$$

The coherence matrix $\hat{T}$ is obtained by multiplying the measurement M matrix with its transposed complex conjugate (denoted as †) and dividing by the number of measurements.

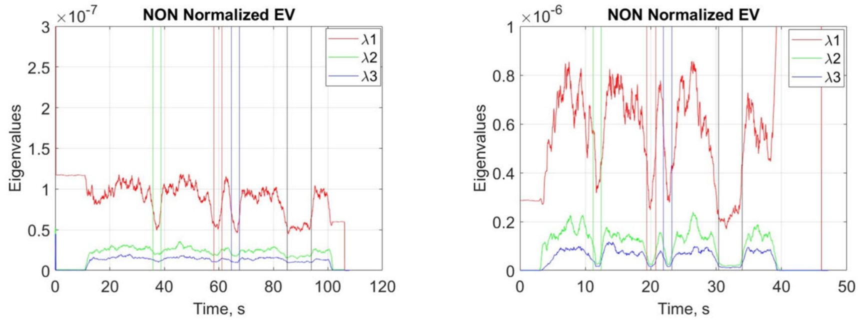

(a) EV for dry/icy surfaces at incidence angle of 60^0. The vehicle is moving with a speed of 3.4 m/s, between 10 and 100s. The ice patches are marked with vertical lines.

(b) EV for dry/wet surfaces at incidence angle of 40^0. The vehicle is moving with a speed of 8.3 m/s, between 3 and 39s. The wet patches are marked with vertical lines.

Fig. 5 Eigen values vs. time for dry, icy, and wet surfaces. All time instances when the vehicle transits from one surface to the other are derived from the video camera and are denoted as vertical lines

$$\hat{T} = \frac{MM^{\dagger}}{N} \tag{5}$$

The coherence matrix can also be represented through its eigenvalues and eigenvectors.

$$\hat{T} = \lambda_1 \left[e_1.e_1^{\dagger} \right] + \lambda_2 \left[e_2.e_2^{\dagger} \right] + \lambda_3 \left[e_3.e_3^{\dagger} \right] \tag{6}$$

where e_i are the 3 elements column eigen-vectors and λ_i are the corresponding eigenvalues. e_i and λ_i are calculated for each range cell and averaged only over those range cells, where the radar beam intersects with the surface. These range cells can be identified from looking at the magnitude of the $[S]$ parameters as shown in Fig. 4. However, a better way is to look at the PP vs. range when the vehicle is not in motion. In this case, all PP should be at 0 value as the surface is measured at the same spot and thus does not appear as random. This is illustrated in Fig. 7 for a static vehicle. The surface location is indicated with vertical lines.

An example of measured eigenvalues is given in Fig. 5 for dry/icy and dry/wet surfaces. An interpretation of the physical meaning of the eigenvalues can be found in [10]. In the context of this paper, we can say that the first eigenvalue λ1 is related to scattering from the surface, while λ2 and λ3 are associated with higher-order scattering from below the surface. This statement is supported by the observation that the highest contrast between dry/icy and dry/wet surfaces is found in λ1 as shown in Fig. 5.

For the dry/icy measurement (Fig. 5a), the angle of incidence is 60°, while for the dry/wet measurement, the incidence angle is 40°, which explains the higher eigenvalues in Fig. 5b

The eigenvalues and the PP in the following figures show variations even when the radar is moving along a uniform dry surface. These variations are caused by the surface itself and are not a result of noise in the radar or low SNR. This can be seen at the beginning and at the end of each sequence where the vehicle is not moving. In

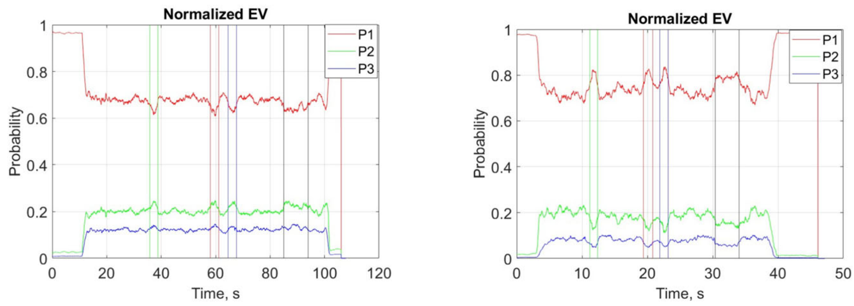

(a) Normalized EV for dry/icy surfaces. The ice patches are marked with vertical lines.

(b) Normalized EV for dry/wet surfaces. The wet patches are marked with vertical lines.

Fig. 6 Eigen values vs. time for dry, icy, and wet surfaces. All time instances when the vehicle transits from one surface to the other are derived from the video camera and are denoted as vertical lines

this case, the first eigenvalue $\lambda 1$ or P1 or any of the PP are constant and do not change with time.

3.1 Normalized EV

The normalized eigenvalues Pi are given in Eq. 7 and have a meaning of probability. P_i represents the relative importance of the corresponding eigenvalue with respect to the total scattered power.

$$P_i = \frac{\lambda_i}{\lambda_1 + \lambda_2 + \lambda_3} \tag{7}$$

Figure 6 shows the normalized eigenvalues for the same dry/ice and dry/wet data as in Fig. 5. Presence of ice on the surface reduces $P1$ and enhances $P2$ and $P3$ as seen in Fig. 6a. This is expected as the ice dielectric constant is not dramatically different from the asphalt and thus it acts as a "matching" layer reducing the contribution of surface scattering $P1$, while enhancing relative scattering from below the surface. For the case of wet patches in Fig. 6b $P1$ is changed in the opposite direction: more surface scattering combined with less penetration into the volume of the surface (lower $P2$ and $P3$). This is because the dielectric constant of water is very much different from the asphalt and thus acts as a "partial" mirror (see Table 3).

3.2 Entropy

Entropy is a measure of the randomness of the scattering process and has a value of 0 for a single non-random target and 1 for a highly random distributed target where several scattering mechanisms are involved. After decomposition of the coherence

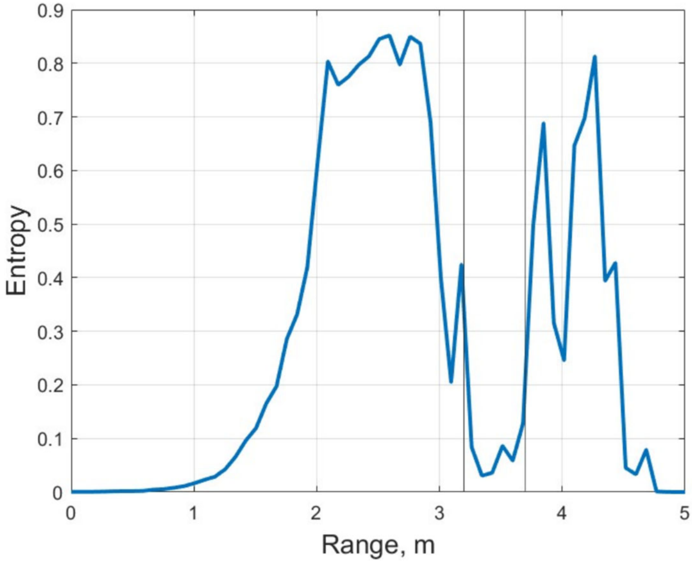

Fig. 7 Entropy vs. range, for static (non-moving) vehicle. In this case, the surface is measured at the same spot and thus does not appear as random; hence, entropy is expected to be 0 for the range cells covering the road surface. The range to the surface appears to be between 3.2 and 3.7m and is marked with vertical lines. This range is consistent with what is expected from the geometry of the radar beam shown in Fig. 3 for 60° angle of incidence

matrix, as shown in Eq. 6, the entropy is calculated from the 3 eigenvalues [4] as shown in Eqs. 7 and 8.

$$H = -\sum_{i=1}^{3} P_i \,.\, \log_3(P_i) \tag{8}$$

An example of Entropy vs. range for a static vehicle is shown in Fig. 7. We expect the Entropy to be 0 for a non-moving vehicle as S-parameters are collected from the same spot on the surface (no independent sampling of the surface), causing the rank of the coherence matrix to collapse to 1 and thus only the first eigenvalue $\lambda 1$ is non-zero (see Figs. 5 and 6). The figure shows that for a range around 3.5m where the radar beam intersects the surface, the SNR is sufficient and the noise in the radar is not a limiting factor; otherwise, the Entropy would not be 0. For range<3 and >3.7m, there is no object, only noise, thus the entropy is approaching its maximum value. For all the PP, an average value is calculated for the range cells covering the surface.

The entropy for dry/icy and dry/wet surfaces is shown in Fig. 8 and is derived for the same data as in Figs. 5 and 6.

So far, we have seen that the dominant scattering mechanism is the backscatter from the surface. Ice-covered surfaces decrease the relative contribution of surface scattering. Entropy, therefore, increases for ice-covered surfaces compared to the same surface in dry conditions. For the case of a wet surface, the relative surface scattering is enhanced compared to its dry condition, resulting in decreased entropy.

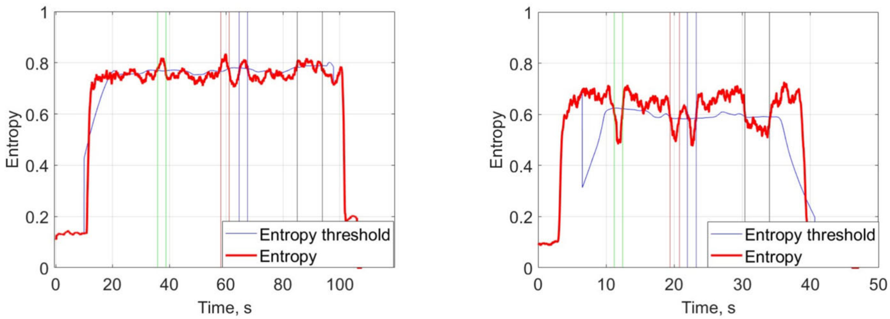

(a) Entropy for dry/icy surfaces (b) Entropy for dry/wet surfaces

Fig. 8 Entropy values vs. time for dry-icy surfaces. The ice/wet patches are marked with vertical lines

3.3 Depolarization

The degree of depolarization generated by the target is another polarimetric parameter given by [9] as:

$$P_H = \frac{min(\lambda 1, \lambda 2, \lambda 3)}{max(\lambda 1, \lambda 2, \lambda 3)} \tag{9}$$

The depolarization, also called polarimetric pedestal for dry/icy and dry/wet surfaces, is shown in Fig. 9 and is derived for the same data as in Fig. 5 and 6. It can be seen that P_H produces higher contrast between dry/icy conditions, but also has larger variations for the dry regions. This can be explained by the presence of $\lambda 3$ in the denominator, which accounts for scattering from below the surface.

3.4 Sum of Eigenvalues

The sum of non-normalized eigenvalues $\Sigma\lambda i$ shown in Fig. 10 has the meaning of total received backscattered power. Although the $\Sigma\lambda i$ provides the highest contrast in the transitions dry/icy and dry/wet, it is apparent that both icy and wet patches reduce the

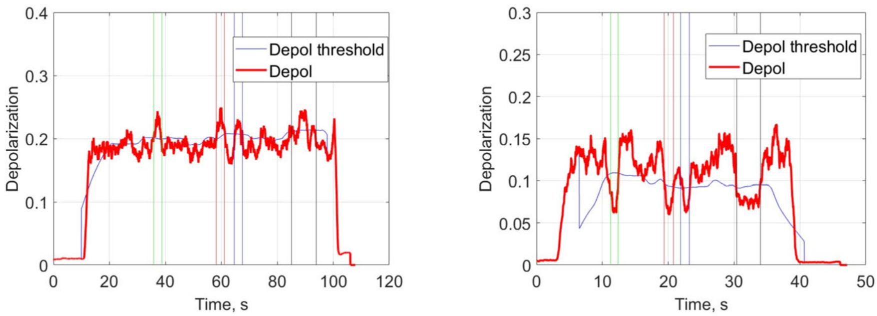

(a) Depolarization for dry/icy surfaces (b) Depolarization for dry/wet surfaces

Fig. 9 Depolarization P_H vs. time for dry-icy surfaces. The ice patches are marked with vertical lines

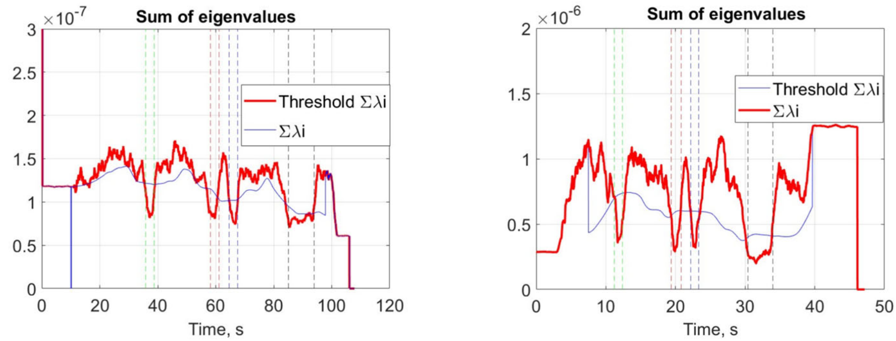

(a) Sum of EV for dry/icy surface (b) Sum of EV for dry/wet surface

Fig. 10 Sum of eigenvalues vs. time. The locations of ice/wet patches are marked with vertical lines

backscattered power. Therefore, $\Sigma\lambda i$ is ambiguous and is not sufficient to distinguish icy from wet areas on its own. However, it can be combined with other PP such as entropy, depolarization, or P1, to reduce the false alarm rate, as shown in the following section.

3.5 Auxiliary Angle α

The mean polarimetric scattering angle α is another parameter used to characterize surfaces [4]. It is calculated, as shown in Eq. 10, from the normalized EV Eq. 7 and the first element of each of the eigenvectors from Eq. 6.

$$\alpha = \sum_{i=1}^{3} P_i.acos(|e_{i1}|) \tag{10}$$

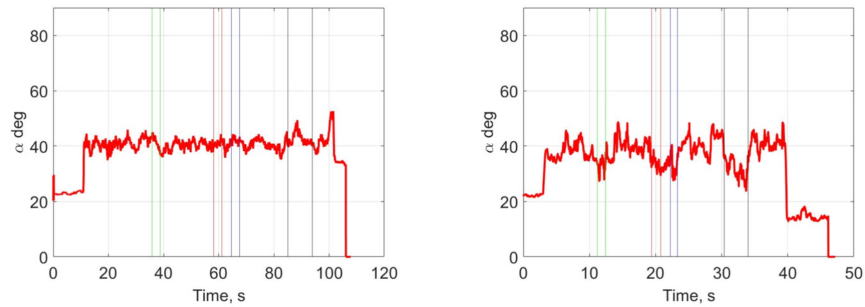

(a) Auxiliary angle α for dry/icy surface. (b) Auxiliary angle α for dry/wet surface.

Fig. 11 Auxiliary angle vs. time for dry, icy, and wet surfaces. The ice/wet patches are marked with vertical lines

The auxiliary angle according to Eq. 10 is shown in Fig. 11 again for dry/icy and dry/wet surfaces (same data as above).

In the context of polarimetric measurements, α indicates the dominant scattering mechanism as follows:

- $\alpha = 0^0$ surface scattering only
- $\alpha = 45^0$ dipole/volume scattering
- $\alpha = 90^0$ double bounce scattering

Based on the measured auxiliary angle presented in Fig. 11, our conclusion is that α does not provide notable contrast in the context of dry/icy/wet classification of the surface, especially in the case of icy surface as in Fig. 11a. For the case of a wet surface, Fig. 11b α decreases in the wet areas, but still the contrast is not as good as the entropy, depolarization, and the first eigenvalue $P1$. Therefore, in regard to this particular application, α is not a good measure of the surface condition and will not be considered for the classification presented in the next section.

4 Classification of the Surfaces

From the previous section, it can be seen that not all polarimetric parameters experience high contrast when transiting from dry to icy or wet surfaces. Generally, dry-wet interfaces show better contrast due to the higher difference between their dielectric constants, as shown in Table 3, compared to dry-icy transitions.

The parameter showing the highest contrast is the first normalized eigenvalue $P1$ from Fig. 6, followed by the depolarization from Fig. 9 and entropy Fig. 8. To evaluate the effectiveness of these 3 parameters in distinguishing dry from icy surfaces, we use a simple classification criterion: each value of the PP is compared to a threshold value. Depending on whether a measurement is below or above its corresponding threshold values, the surface is classified as dry, wet, or icy. To establish the threshold values, we calculate the mean value μ and the standard deviation σ of a set of past measurements over time intervals as illustrated in Fig. 12. These time intervals are varying parameters and depend on the vehicle speed and the size of the patches we are interested in. μ and σ are updated with each measurement point, resulting in adaptive threshold values.

Due to the lower contrast in the case of the icy surface, we add 1/2 standard deviation to the mean value, while for the wet surface, we subtract 0.7 standard deviation as shown in Eq. 11. These threshold values are chosen so that we get a balance between minimum false alarms and missed detections. The resulting threshold values are shown in Fig. 8, 9, and 10.

$$\begin{aligned} threshold(icy) &= \mu + 0,5\sigma \\ threshold(wet) &= \mu - 0,7\sigma \end{aligned} \tag{11}$$

Table 3 Dielectric constant of asphalt, ice, and water at 90GHz according to [12]

Dry Asphalt	Ice	Water
6–0.52.i	3.18–0.007i	6.6–8.7i

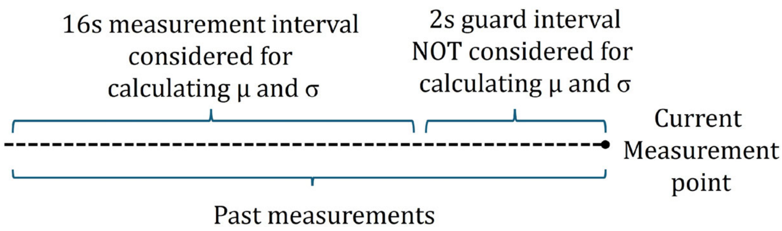

Fig. 12 Illustration of how μ and σ are calculated

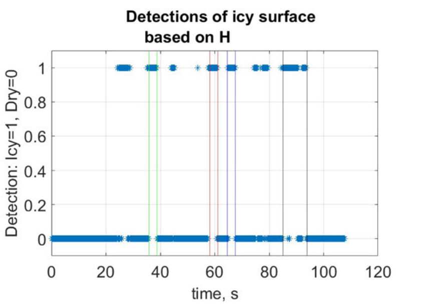

(a) Detection of icy surface based only on the Entropy from Fig. 8a. The figure corresponds to the first column in Table 4.

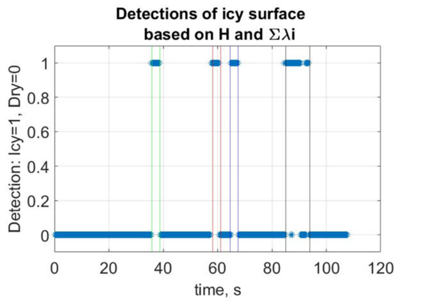

(b) Detection of icy surface based on combination Entropy (Fig. 8a) and sum on the eigenvalues $\Sigma\lambda i$ (Fig. 10a). The figure corresponds to the 4_{th} column in Table 4.

Fig. 13 Detection of icy patches vs. time. Points classified as ice receive a value of 1, while dry surfaces maintain a value of 0. The ice patches are marked with vertical lines

Table 4 False alarm (FA) and missed detection (MD) for dry/icy surfaces

	Entropy H	Depol P_H	EV $P1$	$H+\Sigma\lambda i$	$P_H+\Sigma\lambda i$	$P1+\Sigma\lambda i$
FA, %	15	16	13	1.5	0.6	1.6
MD, %	14	30	14	18	34	18

Table 5 False alarm (FA) and missed detection (MD) for dry/wet surfaces

	Entropy H	Depol P_H	EV $P1$	$H+\Sigma\lambda i$	$P_H+\Sigma\lambda i$	$P1+\Sigma\lambda i$
FA, %	1.4	0.9	3.7	0	0.2	0.1
MD, %	4.4	1.6	3.7	7.4	5	9.8

For example, if measured entropy is above $\mu + 0,5\sigma$ the point is classified as icy, if it is below $\mu - 0,7\sigma$, it is classified as wet. False alarm (FA) and missed detection (MD) are calculated by comparing each classified measurement point to the actual state of the surface, which is derived from a video camera mounted on the vehicle next to the radar and pointed to the surface intersection with the radar beam. Figure 13 compares the output of the surface classification to the actual state of the surface. For example, in Fig. 13a, only the entropy is used for classification, where points exceeding $H > threshold[H(icy)]$ are classified as ice, producing 15% of false alarms and 14% of missed detections. If entropy is combined with the sum of the eigenvalues from Fig. 10a, the FA is reduced to 1.5%. In this case, the condition for a point to be classified as icy is: if $H > threshold[H(icy)]$ and if $\Sigma\lambda i > threshold[\Sigma\lambda(icy)]$.

The sum of the eigenvalues, which produces the highest contrast, can be combined with entropy, depolarization or $P1$ to eliminate the ambiguity in $\Sigma\lambda i$ and reduce the FA rate. Table 4 summarizes the FA and MD in the detection of ice for the major PP and their combination with $\Sigma\lambda i$. Table 5 gives FA and MD in the case of wet areas.

5 Discussion

We present for the first time the detection of ice formations on a road surface using a mono-static polarimetric radar installed on a vehicle in motion. Polarimetric parameters (PP) such as entropy, depolarization, and the eigenvalue representing the surface scattering ($P1$) are used to identify the surface and classify it as dry, wet, or ice. Icy surfaces decrease the first normalized eigenvalue $P1$ and thus increase entropy and depolarization (polarimetric pedestal), while wet surfaces change the parameters above in the opposite direction. The best contrast is found in the sum of the non-normalized EV, which can be used in combination with the aforementioned PP to reduce the false alarm rate. The FA and MD values presented in Table 4 suggest that Entropy or a combination of the first normalized eigenvalue and the sum of the non-normalized eigenvalues $\Sigma\lambda i$ produce a reasonable balance between FA and MD for the case of icy surfaces.

The measurements presented in this paper were performed on a uniform asphalt surface of an airfield. On public roads, other surface parameters such as roughness, presence of pot holes, depressions in the surface, marking lines, and other irregularities will affect all the parameters treated in this work. Therefore, it is not feasible to establish fixed detection threshold values. We suggest using dynamic-threshold, which is updated for each measurement point based on previously measured values. The threshold values can be adapted to the mean value and the standard deviation calculated from the preceding measurements.

In the measurements presented, we perform the processing on a laptop computer, which receives a measurement frame containing the polarimetric scattering parameters each 25 ms. Faster measurements will allow us to use a larger set of measurements for estimating the PP and thus less variations caused by the randomness of the surface. This is possible if the estimation algorithm is implemented in the radar's DSP block. In this case, the amount of data transmitted from the radar will be dramatically reduced, which will allow to detect smaller ice/wet patches at higher vehicle speeds.

Acknowledgements Authors would like to thank the team at Magna Electronics in Vårgårda/Sweden and in particular to Oliver Brunnegård for the support during the measurement campaign. This work is supported by Sweden's innovation agency Vinnova within the program "Strategic vehicle research and innovation." The development of the polarimetric radar is partly financed by VVWaves AB, Lindome, Sweden.

Author Contributions The research presented is carried out mainly by Vessen Vassile. August Kälvesten and Nils Kalmnäs Drakenfors were my students at Chalmers. Their contribution is in writing the software and firmware for the real-time processing. My company VVWaves contributed in the development of the sensor.

Funding Open access funding provided by Chalmers University of Technology. This work is supported by Sweden's innovation agency Vinnova within the program "Strategic vehicle research and innovation."

Data Availability No datasets were generated or analysed during the current study.

Declarations

Ethical Approval Not applicable.

Competing Interests The authors declare no competing interests.

Open Access This article is licensed under a Creative Commons Attribution 4.0 International License, which permits use, sharing, adaptation, distribution and reproduction in any medium or format, as long as you give appropriate credit to the original author(s) and the source, provide a link to the Creative Commons licence, and indicate if changes were made. The images or other third party material in this article are included in the article's Creative Commons licence, unless indicated otherwise in a credit line to the material. If material is not included in the article's Creative Commons licence and your intended use is not permitted by statutory regulation or exceeds the permitted use, you will need to obtain permission directly from the copyright holder. To view a copy of this licence, visit http://creativecommons.org/licenses/by/4.0/.

References

1. N. Kees, J. Detlefsen, "Road surface classification by using a polarimetric coherent radar module at millimeter waves", *IEEE MTT-S International Microwave Symposium Digest*, May 1994.
2. V. Viikari, "Road-Condition Recognition Using 24-GHz Automotive Radar", *IEEE Transactions on Intelligent Transportation Systems, Vol. 10, No. 4*, December 2009.
3. J. Häkli et al., Road surface condition detection using 24 GHz automotive radar technology, *in Proc. 14th Int. Radar Symp. (IRS)*, vol. 2, Jun. 2013, pp. 702–707.
4. S. H. Cloude, "An Entropy Based Classification Scheme for Land Applications of Polarimetric SAR", *IIEEE Transactions on Geoscience and Remote Sensing*, (vol. 35), Jan. 1997.
5. T. Jagdhuber, et. al, "Identification of Soil Freezing and Thawing States Using SAR Polarimetry at C-Band", *Remote Sens.* 2014.
6. A. Babu, S. Baumgartner,"Road Surface Quality Assessment Using Polarimetric Airborne SAR", *IEEE Radar Conference*, Sept. 2020.
7. V. Vassilev, "Road surface recognition at mm-wavelengths using a polarimetric radar", *IEEE Transactions on Inteligent Transportation Systems*,Vol. 23, Issue: 7, July 2022.
8. V. Vassilev, "Road surface characterization using a 77-81 GHz polarimetric radar", *IEEE Transactions on Inteligent Transportation Systems*,Vol. 25, Issue: 9, September 2024.
9. S.L. Durden, et. al.,"The unpolarized component in polarimetric radar observations of forested areas", *IEEE Transactions on Geoscience and Remote Sensing (Volume: 28 , Issue: 2*, Mar 1990.
10. Ulaby, "Microwave radar and radiometric remote sensing", *The University of Michigan Press*, 2014.
11. W. Bouwmeester, F. Fioranelli and A. G. Yarovoy, Road Surface Conditions Identification via H α A Decomposition and its Application to mm-Wave Automotive Radar, *IEEE Transactions on Radar Systems*, Vol. 1, 2023.

12. Olivier Auriacombe; Vessen Vassilev, “Recognition of Road Surface Conditions With a 82–98 GHz Total Power Dual-Polarized Radiometer on a Vehicle”, *IEEE Transactions on Intelligent Transportation Systems* , Vol. 26, 2025.

Publisher's Note Springer Nature remains neutral with regard to jurisdictional claims in published maps and institutional affiliations.